



ELSEVIER

Marine Geology 211 (2004) 21–43

**MARINE
GEOLOGY**

INTERNATIONAL JOURNAL OF MARINE
GEOLOGY, GEOCHEMISTRY AND GEOPHYSICS

www.elsevier.com/locate/margeo

Variations in terrigenous dilution in western Mediterranean Sea pelagic sediments in response to climate change during the last glacial cycle

B.A.A. Hoogakker^{a,*}, R.G. Rothwell^{a,1}, E.J. Rohling^{a,2}, M. Paterne^{b,3}, D.A.V. Stow^{a,4}, J.O. Herrle^{a,5}, T. Clayton^{a,6}

^aSouthampton Oceanography Centre, Empress Dock, Southampton SO14 3ZH, United Kingdom

^bLaboratoire des Sciences du Climat et de l'Environnement, Laboratoire mixte CNRS-CEA, Domaine du CNRS, Avenue de la Terrasse, Gif sur Yvette 91198, France

Received 23 July 2003; received in revised form 29 June 2004; accepted 19 July 2004

Abstract

Hemipelagic intervals in four giant Calypso piston cores from the Balearic Abyssal Plain (western Mediterranean Sea) were studied in order to determine fluctuations in the supply of terrigenous sediments to the basin during the last 130,000 years and possible climatic modulation of terrigenous sediment and particle flux. Carbonate records from hemipelagic intervals in these cores display distinct 'Atlantic' type cycles, where glacial periods show, on average, 20% lower calcium carbonate contents than interglacial period equivalents. The decrease in calcium carbonate seen during glacials may be the result of increased dilution by terrigenous (aeolian and fluvial) particles derived from aeolian and/or fluvial sources. Higher glacial aeolian particle fluxes to the western Mediterranean Sea may have been caused by changes in the prevailing atmospheric conditions, resulting in drier and colder climatic conditions in the source areas and more frequent and intense outbreaks of dust transport. The colder and drier climatic conditions in combination with a lowered sea level would allow rivers to dump their sediment load closer to the shelf edge, promoting enhanced fluvial input into the basin. Besides significant calcium carbonate variations that correlate with glacial/interglacial cycles, several short-term abrupt changes in the calcium carbonate content are recorded, which appear

* Corresponding author. Present address: Department of Earth Sciences, Cambridge University, Downing Street, Cambridge CB2 3EQ, United Kingdom. Tel.: +44 1223 33452; fax: +44 1223 33450.

E-mail addresses: bhoo03@esc.cam.ac.uk (B.A.A. Hoogakker), rgr@soc.soton.ac.uk (R.G. Rothwell), ejr@soc.soton.ac.uk (E.J. Rohling), Martine.Paterne@lsce.cnrs-gif.fr (M. Paterne), davs@soc.soton.ac.uk (D.A.V. Stow), jens.herrle@soc.soton.ac.uk (J.O. Herrle), tc1@soc.soton.ac.uk (T. Clayton).

¹ Tel.: +44 2380 596567; fax: +44 2380 596554.

² Tel.: +44 2380 593042; fax: +44 2380 593059.

³ Tel.: +33 169 823567; fax: +33 169 823568.

⁴ Tel.: +44 2380 593049; fax: +44 2380 593052.

⁵ Tel.: +44 2380 596449; fax: +44 2380 593052.

⁶ Tel.: +44 2380 592003; fax: +44 2380 593052.

0025-3227/\$ - see front matter © 2004 Elsevier B.V. All rights reserved.

doi:10.1016/j.margeo.2004.07.005

coincident with enhanced magnetic susceptibility values, especially the events within Marine Isotope Stage (MIS) 3. The timing of these short-term events may be linked with cooling events in the North Atlantic, particularly Heinrich Events and cold events within MIS 5. These short-term trends may possibly be explained by increased terrigenous particle transport, due to drier and colder climate in the Mediterranean borderlands. Our results further show that about 90% of the sedimentary sequence of the Balearic Abyssal Plain consists of turbidites. Generally, these appear not to have caused significant erosion, and an almost complete continuous time stratigraphy is present in the intercalated hemipelagic intervals.

© 2004 Elsevier B.V. All rights reserved.

Keywords: dilution; terrigenous sediment; Western Mediterranean; last glacial cycle; calcium carbonate records

1. Introduction

The Mediterranean Sea is a semi-enclosed basin (Fig. 1) with anti-estuarine circulation. Its general circulation is of halothermal nature, controlled by the strong excess of evaporation over freshwater input and net cooling in the basin. The resultant net buoyancy loss drives surface inflow and subsurface outflow through the Strait of Gibraltar.

The major glacial/interglacial climatic oscillations of the Pleistocene had a large influence on the western Mediterranean environment (Rose et al., 1999). The development of a fixed anticyclone over the north European ice sheet and colder sea surface temperatures (SSTs) during glacial times resulted in colder and drier conditions (Rognon, 1987) and increased seasonality of precipitation over the Mediterranean (Prentice et al., 1992). The present climate in the western Mediterranean is characterised by a high interglacial global sea level, a relatively dense vegetation cover, relatively high infiltration rates, and moderate river discharges (Rose et al., 1999). The glacial western Mediterranean environment, in contrast, was characterised by a low global sea level, open vegetation with large areas of bare ground, and unconsolidated sediments, with soils affected by high physical stresses and highly peaked river discharge regimes (Rose et al., 1999). SST estimates for the Alboran Sea, based on the relative abundances of planktonic foraminifera species, varied considerably between glacial and interglacial periods, with interglacial maximum SST of 20–23 °C and glacial maximum SST of 10–15 °C (González-Donoso et al., 2000). Alkenone-based SST estimates give similar values of ~19 °C during the Holocene and 11–13 °C during the last glacial maximum (Cacho et al., 2001). Recent research (Rohling et al., 1998; Cacho et al.,

1999, 2001; Paterne et al., 1999; Combourieu Nebout et al., 2002) has shown that the western Mediterranean basin was strongly influenced by the millennial-centennial climatic and oceanographic variability in the north Atlantic region during the last glacial period.

The composition of deep-sea sediments reflects the climatic conditions affecting adjacent continental regions, and/or the oceanic and atmospheric circulation at the time of deposition (McManus, 1970; Kolla et al., 1979). For example, a higher proportion of terrigenous material accumulated in the equatorial and tropical Atlantic offshore of West Africa during glacial times compared to interglacial times, due to higher terrestrial influxes associated with higher trade wind intensities (Diester-Haas, 1976). Changes in the supply of terrigenous material to deep-sea sediments can be estimated by determining the proportion of calcium carbonate, since carbonate content in pelagic sediments is inversely related to dilution with terrigenous material (Hays and Perruzza, 1972). Higher carbonate contents in pelagic sediments of interglacial times reflect a low terrestrial input due to reduced trade wind intensities and a general decrease in aridity (Hays and Perruzza, 1972). Conversely, low carbonate contents in glacial pelagic sediments suggest enhanced terrestrial input associated with higher trade wind intensity and enhanced aridity (Hays and Perruzza, 1972). This scenario is supported by studies by Parkin and Shackleton (1973) and Parkin (1974), who showed that the Saharan desert belt expanded southward during glacials.

Larrasoño et al. (2003) obtained a high-resolution proxy record of northern Sahara dust supply into the eastern Mediterranean for the last 3 Ma, based on magnetic susceptibility measurements. They relate dust flux minima, found at times of northern hemisphere insolation/monsoon maxima, to the

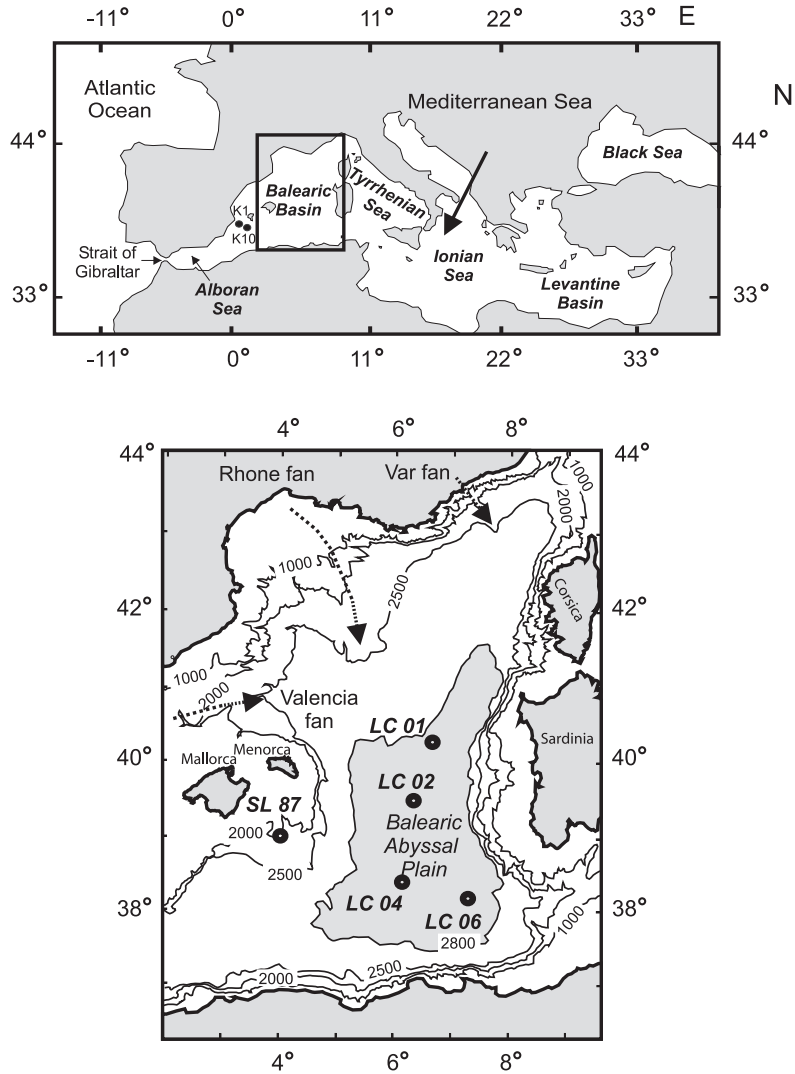


Fig. 1. Map showing the Balearic Abyssal Plain in the western Mediterranean Sea and location of the cores studied (LC01, LC02, LC04, and LC06). The location of SL87 (Weideab et al., 2003), K1, and K10 (Flores et al., 1997) is also shown.

northward penetration of the African summer monsoon front beyond the central Saharan watershed ($\sim 21^\circ\text{N}$). They also argue that such northward penetration of the African summer monsoon correlates with expansion of savannah-like vegetation cover (Claussen et al., 1998; Brovkin et al., 1998) and an increase in the soil cohesiveness throughout the northern Sahara, which resulted in decreased dust production, similar to present conditions in the Sahel (Middleton, 1985).

The western Mediterranean Sea is surrounded by catchment areas subject to continental, alpine, and Mediterranean climate regimes in the north, and Mediterranean to semi-arid climates in the south. During summer, the strong Azores anticyclone dominates the climate over the western Mediterranean basin, whereas during winter, the incursion of north westerlies becomes significant (Sánchez Goñi et al., 2002). At present, northward transport of dust over the Mediterranean is linked to the presence of cyclo-

nes (Moulin et al., 1997) and most Saharan dust deposition over southern Europe is through precipitation (Bücher and Lucas, 1984; Bergametti et al., 1989a,b; Loye-Pilot et al., 1989; Guerzoni et al., 1992). Major source areas of dust transport to Western Europe are Algeria, the Western Sahara, and the Moroccan Atlas (Molinaroli, 1996; Avila et al., 1997; Goudie and Middleton, 2001). Weldeab et al. (2003) use Si/Al and Ti/Al ratios as well as Sr and Nd isotopes to show that the Saharan terrigenous input into the western Mediterranean Sea is predominantly from the southwest (Morocco/NW Algeria) and south-east (Tunisia/West Libya) during interglacial periods, and from the southern Saharan/Sahelian region during glacial times. The change in sediment source reflects changes in the prevailing atmospheric circulation over the basin (Weldeab et al., 2003). Their study also found that glacial terrigenous input was much higher than during interglacial times. A high-resolution record of lithogenic fraction variability from the Alboran Sea shows that millennial-scale to submillennial-scale marine oscillations, linked to Heinrich Events (HEs) and Dansgaard–Oeschger (D/O) stadials, were characterised by increased northward Saharan dust transport due to increased Saharan wind intensity (Moreno et al., 2002).

Here, we discuss the calcium carbonate content of hemipelagic sediment sequences in four giant piston cores from the Balearic Abyssal Plain to determine fluctuations in the supply of terrigenous particles during the last 130,000 years. The derived calcium carbonate records, supported by accelerator mass spectrometry (AMS) radiocarbon dates, biostratigraphy, and oxygen isotope stratigraphy, are used to calculate terrigenous accumulation rates that are compared with accumulation rates reported by Weldeab et al. (2003).

2. Terrigenous particle input into the western Mediterranean Sea

It has been suggested that more than 80% of the total input of terrigenous material (excluding gravity flow deposits) in the western Mediterranean is from Saharan dust (Loye-Pilot et al., 1986; Martin et al., 1989; Guerzoni et al., 1999). Based on $^{143}\text{Nd}/^{144}\text{Nd}$ ratios, the study of Weldeab et al. (2003) shows that

the lithogenic dust fraction of core SL87/KL66 (for location, see Fig. 1) consists mainly of European and Saharan windblown dust. Apart from aeolian dust, the four cores used in this study are likely to have also received suspended matter originating from rivers draining into the western Mediterranean Sea, as they are located in the deeper parts of the Balearic Abyssal Plain. Of these rivers, the Rhône, Ebro, and Var have the largest catchment area and per year they deliver around 16×10^6 tonnes of sediment to the continental margin (Nelson, 1990; Pont, 1993; Mulder et al., 1997). Minor rivers on Corsica, Sardinia, the Balearic Islands, and North Africa only carry small sediment loads, which are unlikely to contribute significantly to the terrigenous input into the basin. It may be possible to distinguish between aeolian and fluvial derived clays in the hemipelagic sediments based on clay mineralogy. Clay minerals from the Rhône and Ebro contain high concentrations of illite and chlorite, both exceeding the amount of kaolinite (Added et al., 1984; Alonso and Maldonado, 1990). Aeolian dust, on the other hand, may be dominated by smectite (if derived from Morocco and western Algeria), or may be rich in kaolinite (if sourced from eastern Algeria/Tunisia and the Saharan area) (Bücher et al., 1983; Bergametti et al., 1989b; Guerzoni et al., 1997).

Magnetic susceptibility measurements are useful in sediment studies because they can be sensitive indicators of temporal variations in the concentration and grain size of terrigenous material deposited on the sea floor (Verosub and Roberts, 1995). Fluctuations in the concentration and size of magnetic grains in deep-sea cores may be climatically modulated (e.g., Amerigian, 1974; Kent, 1982; Oldfield and Robinson, 1985; Bloemendal and DeMenocal, 1989; Robinson et al., 1995). In the North Atlantic, for example, glacial periods are characterised by high concentrations of magnetic minerals, in association with low carbonate contents and increased amounts of ice-rafted detritus. In contrast, sediments from interglacial periods have low magnetic mineral concentrations and high carbonate contents (Robinson, 1986). To test whether a similar relationship (low carbonate content with high magnetic susceptibility intensity during glacials versus high carbonate content with low magnetic susceptibility intensity during interglacials) exists in the western Mediterranean Sea as a result of

variations in the terrigenous particle flux, we compare the derived calcium carbonate and magnetic susceptibility data.

3. Carbonate cycles in the western Mediterranean

The calcium carbonate (CaCO_3) content of deep-sea marine sediments is generally controlled by three factors, assuming that marine plankton remains form the main carbonate component. These factors include: (i) dissolution, (ii) surface water productivity, and (iii) dilution by terrigenous sediments and/or noncarbonate productivity. Van Os et al. (1994) attributed distinctive Pliocene CaCO_3 cycles in the Mediterranean to mainly variations in productivity, combined with dilution by enhanced terrigenous input. Intervals characterised by lower CaCO_3 content showed high organic carbon and Ba (Van Os et al., 1994) and coincided with periods of abundant rainfall on the Mediterranean borderlands (Foucault and Mélières, 2000). Intervals of higher CaCO_3 content are more likely a result of high carbonate productivity (Van Os et al., 1994) formed during more arid conditions (Foucault and Mélières, 2000). Concerning productivity during the Quaternary, Flores et al. (1997) suggest that, after accounting for the dilution factor, production of coccolithophores appears to have been higher during interglacial periods. Weldeab et al. (2003), on the other hand, propose that biomediated barium accumulation rates were highest during glacial periods, indicating enhanced surface water productivity. Bárcena et al. (2001) also suggest increased glacial surface water productivity, as reflected in the high abundance of diatoms found during glacial periods. Both biomediated barium accumulation rates (Weldeab et al., 2003) and diatom abundance (Bárcena et al., 2001) may reflect non-coccolith produc-

tivity. Combined with the data from Flores et al. (1997), this may indicate that carbonate (coccolith) productivity was higher during interglacial times, while non-carbonate (opal, diatoms) productivity was elevated during glacial times.

4. Location and material

The Balearic Abyssal Plain is the largest basin plain in the Mediterranean Sea (Fig. 1) with an area of approximately 77,000 km² (Rothwell et al., 1998, 2000) and is defined by the 2800-m isobath. The Var, Rhône, and Valencia fans bound the plain to the north and northwest, the islands of Corsica and Sardinia to the east, the Balearic rise to the southwest, and the Algerian shelf to the south (Fig. 1). The basin plain's flat morphology is a result of turbidite ponding. These turbidites have a mainly European (Rhône and Var fan) provenance with minor turbidites originating from the African margin (turbidite bases towards the northern part of the basin are thicker and coarser in grain size) (Vanney and Genneseaux, 1985; Bellaiche, 1993; Torres et al., 1997).

Four giant piston cores (LC01, LC02, LC04, and LC06) were recovered from the Balearic Abyssal Plain (Fig. 1, Table 1) during *Marion Dufresne* Cruise 81 in 1995 (under the MAST II PALAE-OFLUX Program), using a Calypso piston corer. The cores, reaching 27–32 m in length, were taken about 100–120 km apart to form an approximate north–south transect across the plain (Fig. 1). Thomson et al. (2000) and Thouveny et al. (2000) have demonstrated that the upper 10–15 m of some Calypso cores can appear to be a factor of 1.5–2 times longer when compared with conventional piston cores from the same site. This difference is due to stretching, oversampling, and a microfabric

Table 1

Location and water depth of the four long piston cores (LC01, LC02, LC04, and LC06)

Core	Latitude	Longitude	Water depth (m)	Core	Latitude	Longitude	Water depth (m)
LC01	40°5.82' N	6°53.23' E	2845	SL87/KL66	38°59.34' N	4°01.40' E	1900
LC02	39°31.88' N	6°22.58' E	2860	K1	38°57.0' N	0°50.0' E	750
LC04	38°39.01' N	6°06.64' E	2855	K10	38°03.0' N	1°00.9' E	1957
LC06	38°00.66' N	7°11.09' E	2845				

Also shown are details of cores SL87 (from Weldeab et al., 2003) and K1 and K10 (from Flores et al., 1997).

rotation in the vertical direction (Thouveny et al., 2000). The lithological units in the Calypso piston cores that are used in this study appear to be anomalously thick in the upper 15 m, and this interval may have been stretched during coring. To reduce this effect, we divided the length of the intervals involved by the maximum stretch factor of two in our study (after Thomson et al., 2000; Thouveny et al., 2000).

All four cores are dominated by sequences of thick, grey, and greyish olive structureless muds (some grading down to basal sands and silts) intercalated with thinner, commonly bioturbated foraminifer-rich mud intervals. The structureless muds and associated silts and sands are interpreted as turbidite deposits on the basis of their organisation and textural character, whereas the foraminifer-rich intervals are interpreted as hemipelagic deposits (Fig. 2). Hemipelagic sedi-

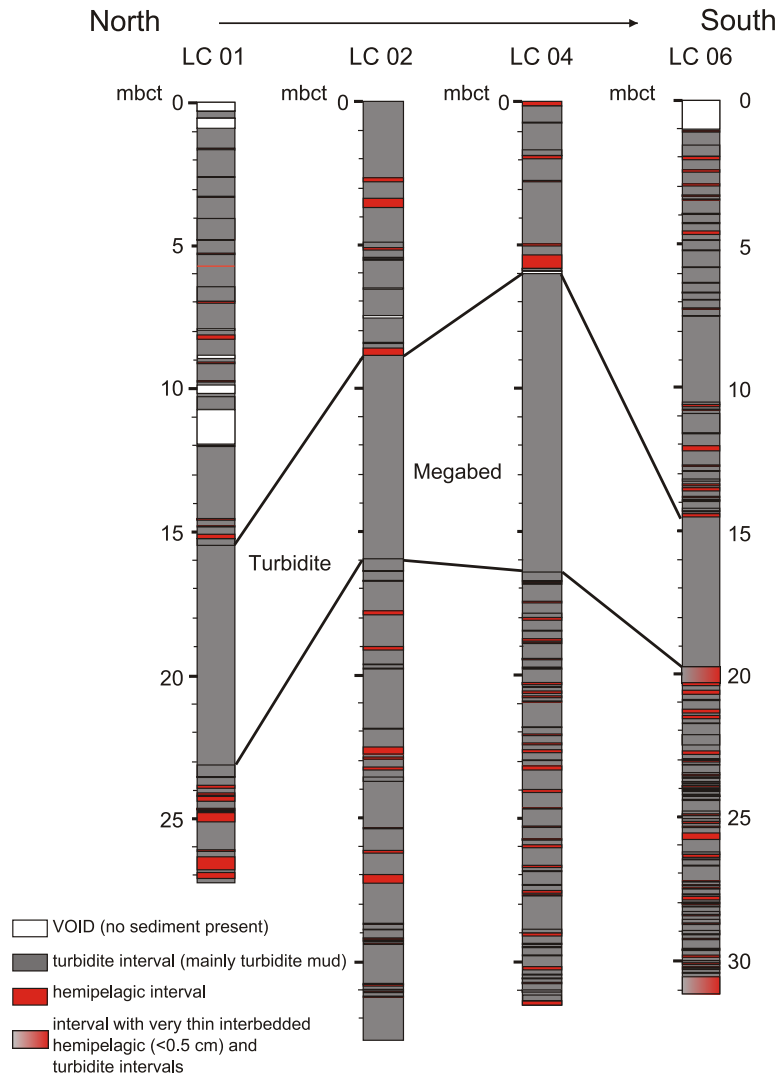


Fig. 2. Turbidite (grey) and hemipelagic (red) intervals identified on sedimentological and textural criteria in the four long piston cores. White intervals delineate voids (i.e., contain no sediment). In core LC06, two intervals occur with very thin (<0.5 cm) hemipelagic and turbidite intervals shown as transitional light–dark grey. Mbct denotes metres below core top. Note that the top 15 m are not corrected for stretching during the coring process. (For colours see online version of this article.)

Table 2

Characteristics of turbidite beds and hemipelagic intervals (after Rupke and Stanley, 1974; Stow and Piper, 1984; Jones et al., 1992; Rothwell et al., 1994; Stow and Tabrez, 1998)

	Hemipelagic units	Turbidites
Bed organisation	The upper boundary between turbidite beds and hemipelagic interval is usually gradational.	The lower boundary between turbidite beds and hemipelagic intervals is generally planar and sharp.
Colour	Colours range from light olive brown (5Y 5/3) to olive grey (5Y 2/2) with subtle variations in hue and chroma over short segments of the core.	Colours range from uniform light olive brown to olive grey.
Bioturbation	Minor to strong mottling occurs due to bioturbation.	Sediment is generally homogenous with bioturbation only occurring in the top 10–20 cm.
Foraminifer distribution	Foraminifera occur scattered throughout the sediment. Underhand lens sediment appears speckled.	Foraminifera are generally rare or absent, except near the base of the turbidite. Underhand lens sediment appears featureless.
Texture	The cut core surface frequently appears pitted.	The cut core surface appears smooth for turbidite muds.
Sedimentary structures	Apart from bioturbation, these are generally absent.	Various sedimentary structures may be observed including normal grading in sand-based turbidites, parallel and wavy lamination (in turbidite mud and silt/sand), cross-lamination, and convolute lamination (in turbidite silt/sand, convolute lamination is normally restricted close to base of turbidites).
Physical properties (wet bulk density, P-wave velocity, and magnetic susceptibility)	Wet bulk density, P-wave velocity, and magnetic susceptibility generally fall within a restricted range, compared to turbidite intervals.	Wide range of measurements for all three properties. Sharp turbidite bases are generally characterised by abrupt changes in all three properties. Grading is commonly observed.

ments are clearly distinguished from turbidite deposits, based on: (1) lack of sharp/planar lower boundaries with turbidite deposits; (2) subtle colour variations; (3) lack of sedimentary structure apart from minor to strong bioturbation; (4) scattered distribution of foraminifera throughout the sediment; and (5) pitted cut core surfaces due to cheese wire drag on the scattered foraminifera when the cores are split (Table 2).

Hemipelagic intervals of the studied Balearic Abyssal Plain cores only make up ~10% of the total sediment thickness (Table 3). Turbidites account for the other ~90% of the sediment column. The total hemipelagic thickness recovered increases from the most northerly core (LC01; 9% of the recovered sediment column) to the southernmost core (LC06; 13% of the recovered sediment column) (Table 3). After correcting the top 15 m for stretching, the total

Table 3

Core	Total sediment thickness (m)	Total thickness of turbidites		Total thickness of hemipelagic intervals	
		m	Percent of total	m	Percent of total
<i>(a) Summary of total thickness of the lithological units appearing in the four cores</i>					
LC01	24.3	22.2	91	2.1	9
LC02	32.5	30.2	93	2.3	7
LC04	31.1	27.7	89	3.4	11
LC06	29.6	25.7	87	3.9	13
<i>(b) Summary of total thickness of the lithological units present in the four cores after correcting for stretching in the upper 15 m of the sediment column</i>					
LC01	18.1	16.4	91	1.7	9
LC02	24.9	23.0	92	1.9	8
LC04	23.4	20.5	88	2.9	12
LC06	22.3	19.1	86	3.1	14

true length of the cores (summed thickness of turbidite and hemipelagic intervals) decreases (Table 3). However, the relative contributions of turbidites and hemipelagic intervals to the total sediment thickness remain unchanged after the correction (Table 3).

In core LC06, two intervals occur with very thinly bedded (<0.5 cm) intercalated hemipelagic and turbidite intervals (Fig. 2). The first interval occurs around 20 m below core top (mbct) and the second at the bottom of the core, up to 30.5 mbct. Because the hemipelagic layers in these intervals are so thin, we were unable to collect sufficient sample for CaCO₃ analysis and the hemipelagic depths are not included in Table 3. In the following sections, the abbreviation THD is used to refer to total hemipelagic depth (i.e., total depth of summed hemipelagic intervals below the core top; i.e., with the turbidites removed).

Hemipelagic accumulation rates measured in nearby cores SL87/KL66 and K1 from the Balearic Island slopes and core K10 from the Algero-Balearic Sea (for location, see Table 1) are reported as around 3–4 cm/ka (Flores et al., 1997; Weldeab et al., 2003).

5. Techniques and methods

5.1. Time-stratigraphic framework

Our time-stratigraphic frameworks for LC01, LC02, LC04, and LC06 are based on the high-resolution nannofossil biozones of Weaver (1983), AMS ¹⁴C dating, oxygen isotope stratigraphy (only for LC01 and LC04), and correlation based on CaCO₃ records. Turbidity currents that deposited on the Balearic Abyssal Plain may have caused erosion of the underlying sediments, thus creating chronostratigraphic discontinuities. In a sufficiently detailed time-stratigraphic framework, major chronostratigraphic discontinuities should show up as hiatuses and can therefore be located. For the Madeira Abyssal Plain, Weaver and Thomson (1993) found that turbidity currents emplaced caused only little—or no—erosion on the plain. Comparison of visual core description with major element X-ray fluorescence (XRF) profiles (unpublished data) of lithological units in core LC06 showed no discrepancies and rules out the possibility of undetected turbidites within the cored sequence.

The planktonic foraminifera *Neogloboquadrina pachyderma* (right coiling or dextral variety) was selected for the stable oxygen and carbon isotope analysis using 15–20 specimens from the 250–400 μm size fraction. *N. pachyderma* occurs virtually continuously throughout the hemipelagic intervals of cores LC01 and LC04. Oxygen and carbon isotope ratios were measured using a Europa GEO 20 20 stable isotope ratio mass spectrometer, with individual acid bath carbonate preparation. Analytical precision of powdered carbonate standards is 0.06‰ for δ¹⁸O and δ¹³C. The stable isotopes are expressed as δ¹⁸O and δ¹³C (‰) relative to the Vienna Pee Dee Belemnite (V-PDB) standard. A total of 42 and 60 samples were analysed for LC01 and LC04, respectively. The δ¹⁸O records are initially divided into the standard δ¹⁸O stages (MIS) following the nomenclature of Emiliani (1955) and Shackleton and Opdyke (1973). The oxygen isotope stages are then further subdivided into substages or events based on Imbrie et al. (1984) and Prell et al. (1986). The time scale of Martinson et al. (1987) was applied for δ¹⁸O stages and events.

CaCO₃ contents were measured by coulometry. Samples were collected from hemipelagic intervals at 2- to 4-cm intervals when sufficiently thick. The top 12–13 m of LC06 appeared disturbed and were therefore not sampled. Samples were thoroughly oven dried at 100 °C. The dried samples were then powdered and CaCO₃ content was measured from CO₂ liberated by reaction with 10% phosphoric acid for 6 minutes. A total of 376 samples were analysed. The analytical precision (standard deviation) for standard bulk sample is 1.50%.

5.2. Sediment mineralogical characteristics

A Bartington MS2EI magnetic susceptibility point sensor was used to measure the magnetic properties of the hemipelagic intervals in the four cores, at 1-cm intervals. The composition of selected hemipelagic intervals was determined by microscopic examination of smear slides, using percentage estimation comparison charts, which allowed the assessment of the relative abundance of detrital (terrigenous) and biogenic grains (Rothwell, 1989).

The clay mineralogy of hemipelagic sediments was determined using X-ray diffraction (XRD). The carbonate fraction of the samples was removed using 1 M

acetic acid. Samples were analysed using an X-ray diffractometer (model Phillips Ultra-Pro) between 2θ angles of $2\text{--}17^\circ$ (air-dried, 375 and 550°C) and $2\text{--}40^\circ$

(glycolated). Intensity peaks were measured using an in-house computer-based mineral identification program (XRDv3; University of Southampton). Clay

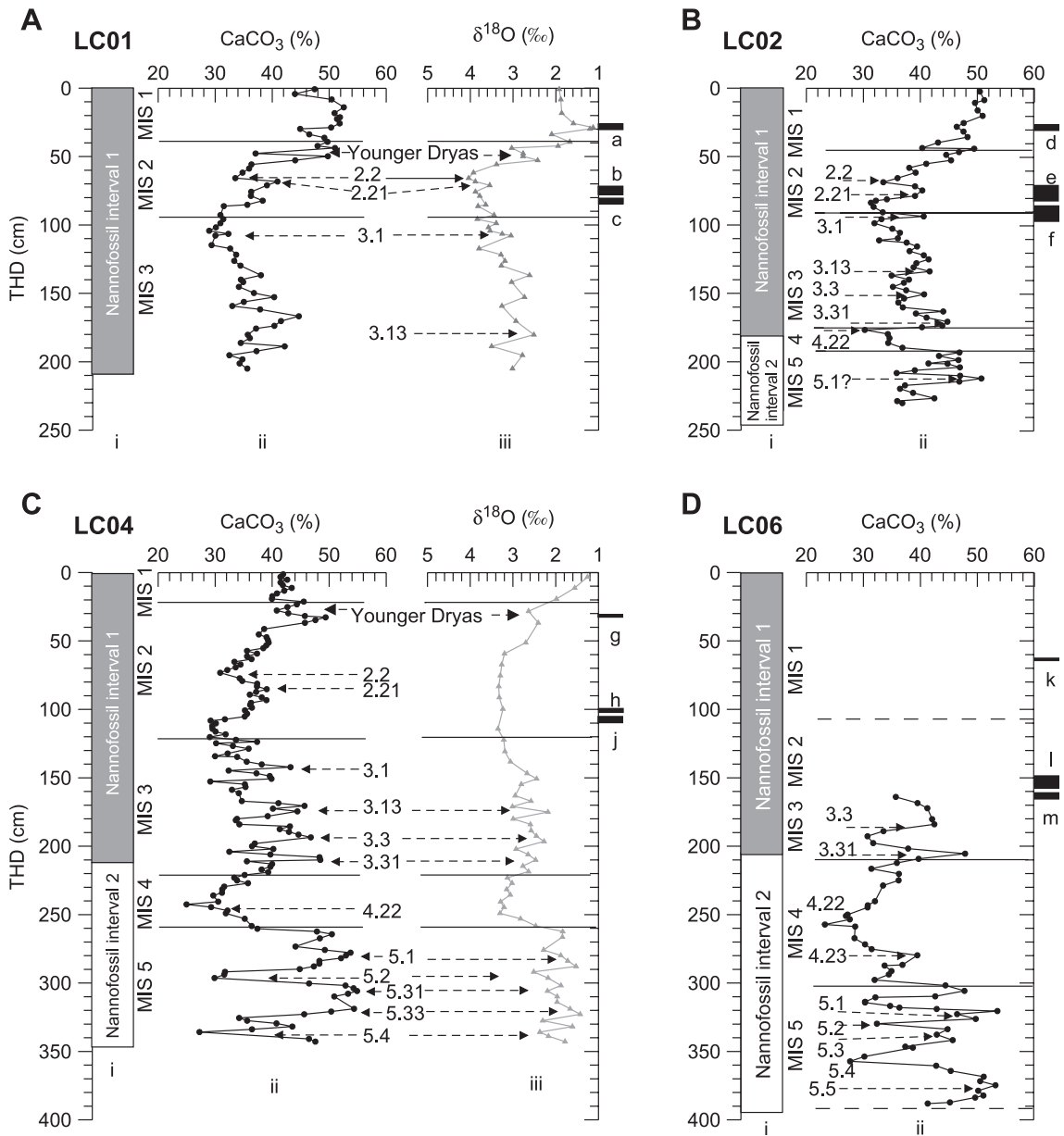


Fig. 3. Time-stratigraphic framework for LC01 (A), LC02, (B), LC04 (C), and LC06 (D) with: (i) Biostratigraphy based on Quaternary nannofossil intervals of Weaver (1983); (ii) calcium carbonate stratigraphy; and (iii) oxygen isotope stratigraphy (only for cores LC01 and LC04) for the summed hemipelagic intervals in the four long piston cores. Nannofossil interval 1 (Weaver, 1983) is shown in black and interval 2 in white. Boundaries of MIS are delineated. Fractional numbers (e.g., 3.1) indicate the position of oxygen isotope events (after Imbrie et al., 1984; Prell et al., 1986). Black boxes at the right side of each graph indicate the sample location of AMS radiocarbon dates. The box thickness corresponds to the thickness of the sampled interval. Radiocarbon ages are reported for each sample (lower case letter) in Table 4.

Table 4
Conventional and calibrated radiocarbon dates for 12 samples (three from each core)

Core	Sample depth (mbct)	Sample number	THD (cm)	¹⁴ C age (years BP±1σ)	Calibrated age (years BP)
LC01	6.95–7.03 ^x	a	26–29.5	8066±47	8445–8573
	14.49–14.61 ^y	b	71–77	17,580±120	19,994–20,674
	23.52–23.63 ^y	c	79.5–85.5	20,340±150	23,092–23,928
LC02	3.56–3.60 ^x	d	26.5–30	9303±49	9833–10,125
	8.72–8.88 ^y	e	70–80.5	16,900±120	19,223–19,879
	17.78–17.93 ^y	f	86.5–97	23,410±210	~26,760 ^z
LC04	1.97–1.99 ^x	g	29–31	11,720±56	13,399–13,403
	5.93–6.23 ^y	h	~102	17,700±130	20,126–20,818
	16.96–17.08 ^y	j	103–107.5	20,200±170	22,919–23,780
LC06	4.66–4.69 ^x	k	62–63.5	7991±43	8381–8481
	14.46–14.65 ^y	l	148–158	17,730±190	20,126–20,886
	20.17–20.19 ^y	m	160.5–165.5	34,380±660	~37,230 ^z

The reported conventional radiocarbon ages were calibrated using INTCAL98 (Stuiver et al., 1998).

^x New dates (this paper).

^y From Rothwell et al. (1998).

^z Samples calibrated using the magnetic curve of Laj et al. (1996).

minerals were identified on the position of their basal spacings and the changes in these spacings after the four treatments (air-dried, glycolated, 375 and 550 °C). Identification was made on the basis of the first (usually the most intense) peak after Brindley and Brown (1980).

6. Results

6.1. Time-stratigraphic framework

A relatively well-constrained time-stratigraphic framework was derived for each of the four cores

(Fig. 3) on the basis of Weaver (1983) nannofossil intervals as identified in Rothwell et al. (1998), AMS radiocarbon dates, and stable oxygen isotope data (for LC01 and LC04 only) for hemipelagic intervals.

Coccolith assemblages in the cores are generally abundant, well preserved, and diverse. The boundary between the Weaver (1983) coccolith intervals 1 and 2, dated ~50,000 years BP, was determined in the cores by Rothwell et al. (1998). Coccolith interval 1 is defined as an interval dominated by *Emiliania huxleyi*. This species is much rarer in interval 2 where *Geophyrocapsa muelleriae* becomes dominant. In LC01, Rothwell et al. (1998) only identified the coccolith stage 1 of Weaver (1983), giving this core a

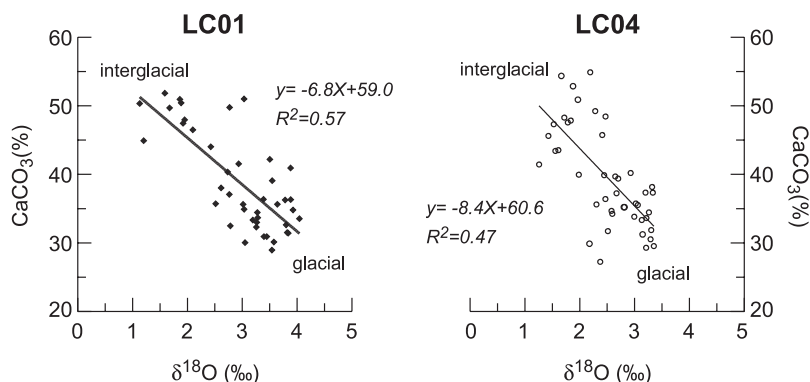


Fig. 4. Linear relationship between $\delta^{18}\text{O}$ and calcium carbonate content in hemipelagic intervals in cores LC01 and LC04.

Table 5

Tie points used for the age models: oxygen isotope stages and events derived from the CaCO₃ and δ¹⁸O records in Fig. 3

Age control points	THD (cm)	Age (ka BP)
<i>Core LC01</i>		
AMS radiocarbon date	28	8.5
Top Younger Dryas/ boundary MIS 1 and MIS 2	43	12.05
Base Younger Dryas	53	12.75
Oxygen isotope event 2.2	66	17.85
Oxygen isotope event 2.21	68	19.22
AMS radiocarbon date	74	20.33
AMS radiocarbon date	83	23.51
Boundary MIS 2 and MIS 3	95	24.11
Oxygen isotope event 3.1	108	25.42
Oxygen isotope event 3.13	181	43.88
<i>Core LC02</i>		
AMS radiocarbon date	28	9.98
Boundary MIS 1 and MIS 2	53	12.15
Oxygen isotope event 2.2	69	17.85
Oxygen isotope event 2.21	74	19.22
Boundary MIS 2 and MIS 3	91	24.11
Oxygen isotope event 3.1	93	25.42
Oxygen isotope event 3.13	133	43.88
Oxygen isotope event 3.3	151	50.21
Oxygen isotope event 3.31	171	55.45
Boundary MIS 3 and MIS 4	175	58.96
Oxygen isotope event 4.22	177	64.09
Boundary MIS 4 and MIS 5	191	73.91
Oxygen isotope event 5.1	212	79.25
<i>Core LC04</i>		
AMS radiocarbon date	30	13.40
Oxygen isotope event 2.2	73	17.85
Oxygen isotope event 2.21	86	19.22
AMS radiocarbon date	~102	20.47
AMS radiocarbon date	105	23.35
Boundary MIS 2 and MIS 3	122	24.11
Oxygen isotope event 3.1	142	25.42
Oxygen isotope event 3.13	172	43.88
Oxygen isotope event 3.3	195	50.21
Oxygen isotope event 3.31	211	55.45
Boundary MIS 3 and MIS 4	221	58.96
Oxygen isotope event 4.22	244	64.09
Boundary MIS 4 and MIS 5	261	73.91
Oxygen isotope event 5.1	279	79.25
Oxygen isotope event 5.2	298	90.95
Oxygen isotope event 5.31	307	96.21
Oxygen isotope event 5.33	320	103.29
Oxygen isotope event 5.4	337	110.79
<i>Core LC06</i>		
AMS radiocarbon date	63	8.43
AMS radiocarbon date	153	20.51

Table 5 (continued)

Age control points	THD (cm)	Age (ka BP)
<i>Core LC06</i>		
AMS radiocarbon date	163	~37.23
Oxygen isotope event 3.3	184	50.21
Oxygen isotope event 3.31	205	55.45
Boundary MIS 3 and MIS 4	210	58.96
Oxygen isotope event 4.22	257	64.09
Oxygen isotope event 4.23	281	68.83
Boundary MIS 4 and MIS 5	300	73.91
Oxygen isotope event 5.1	321	79.25
Oxygen isotope event 5.2	330	90.95
Oxygen isotope event 5.3	338	99.38
Oxygen isotope event 5.4	357	110.79
Oxygen isotope event 5.5	375	123.82
Boundary MIS 5 and MIS 6	388	129.84

AMS radiocarbon dates were used where midpoints were taken from hemipelagic depths and ages. Some AMS radiocarbon ages were not used as they covered a too-long depth interval.

maximum age of ~50,000 years BP (Fig. 3). In LC02, LC04, and LC06, coccolith intervals 1 and 2 were identified, suggesting that these cores penetrate to levels older than 50,000 years BP (Fig. 3).

Rothwell et al. (1998) reported eight radiocarbon dates for hemipelagic intervals that bracket a Late Pleistocene megaturbidite present in all four cores (Table 4). We obtained four additional radiocarbon dates (Table 4). All are based on clean handpicked planktonic foraminifera and pteropods from the >150-μm size fraction. The reported radiocarbon convention ages were calibrated using INTCAL 98 (Stuiver et al., 1998). Two radiocarbon convention ages of 23,410 and 34,380 were calibrated for variations in geomagnetic field intensity using the curve of Laj et al. (1996). Calibrated radiocarbon dates (Table 4) are shown in Fig. 3 as black boxes, where the thickness of the box illustrates the thickness of the hemipelagic sample for radiocarbon analysis. Most samples were obtained from selected hemipelagic intervals, except for 'h,' where foraminiferal tests from bioturbated turbidite mud underlying a hemipelagic interval (T₈ bioturbated turbidite mud; Stow and Shanmugam, 1980) were also used (Rothwell et al., 1998). The THD used for this sample corresponds to the 'bottom' of the overlying hemipelagic interval.

Oxygen isotope measurements were made only for LC01 and LC04 (Fig. 3). In LC01, Marine Isotope Stage (MIS) 1, MIS 2, and (part of) MIS 3 are present. LC04 covers the interval from MIS 5 to the base of MIS 1. To establish a tight chronostratigraphy, we have also indicated isotopic substages and events, based on Imbrie et al. (1984) and Prell et al. (1986) (Fig. 3).

Calcium carbonate percentages are plotted against THD in Fig. 3. The CaCO_3 (%) and oxygen isotope records of LC01 and LC04 show a strong correlation, suggesting that CaCO_3 (%) records recovered from the Balearic Abyssal Plain mimic the oxygen isotope records, with high CaCO_3 (~45–50%) intervals correlating with interglacial stages (MIS 1 and MIS 5); intermediate-value CaCO_3 (~35–45%) intervals with MIS 3; and low CaCO_3 (~25–35%) intervals with glacial stages (MIS 2 and MIS 4) (Figs. 3 and 4). The observed relationship between the CaCO_3 and oxygen isotope records suggests that CaCO_3 variations can be used as a stratigraphic proxy for the Quaternary hemipelagic sediments of the western Mediterranean basin.

Depth–age profiles, based on variously defined age control points (Table 5) for the four cores, indicate a stable background sedimentation (Fig. 5). The stretched upper 15 m of the four cores, involving THDs of 0–0.74 m in LC01, 0–0.80 m in LC02, 0–1.02 m in LC04, and 0–1.58 m in LC06, were corrected by dividing the respective hemipelagic intervals by the maximum stretch factor of two, which resulted in a slight decrease in the background sedimentation rates,

from 3.2 to 2.7 cm/ka after correction (Fig. 5). These accumulation rates are broadly comparable to accumulation rates of 3–4 cm/ka measured in cores from the Balearic Island slopes (Flores et al., 1997) and the Algero-Balearic Sea (Weldeab et al., 2003). Our combined stratigraphy results in an average sample resolution of ~0.8 ka. Based on the various age control points (Table 5), sample depths were converted to age (ka BP) through linear interpolation, allowing records to be presented against age (Fig. 6). We consider it unlikely that turbidity currents caused large-scale erosion of hemipelagic intervals in the four cores studied here, but it cannot be excluded that small-scale erosion features have gone undetected.

6.2. Sediment mineralogical characteristics

Magnetic susceptibility records are plotted alongside the CaCO_3 percent records in Fig. 6. Interglacial intervals, characterised by high CaCO_3 contents, generally have lower magnetic susceptibility values, whereas glacial periods with low CaCO_3 contents show enhanced magnetic susceptibility values (Fig. 6). Apart from these long-term trends, several short-term low CaCO_3 content intervals can be identified, which coincide with short-term increases in magnetic susceptibility in the four cores (Fig. 6).

Smear slide examination of hemipelagic intervals shows that all samples contain a substantial biogenic component (mainly coccoliths, foraminifera, and foraminifer fragments) as well as a terrigenous

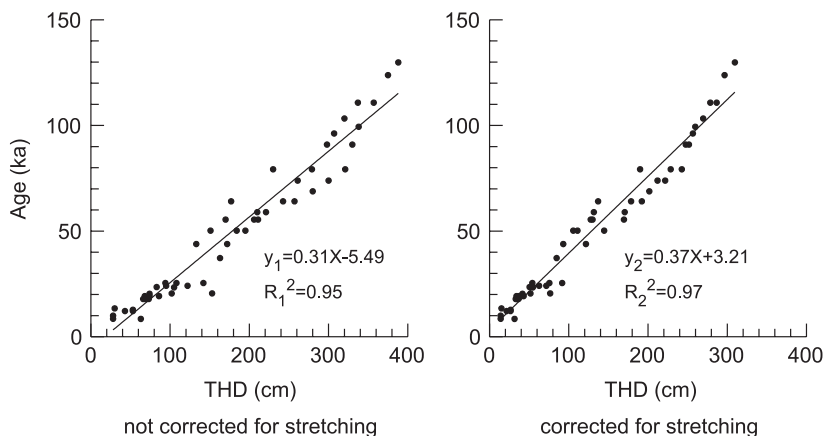


Fig. 5. Depth–age profile through all age control points (Table 5). The linear regression indicates a stable background sedimentation, which shows an overall slight decrease (from 3.2 to 2.7 cm/ka) after correction for stretching.

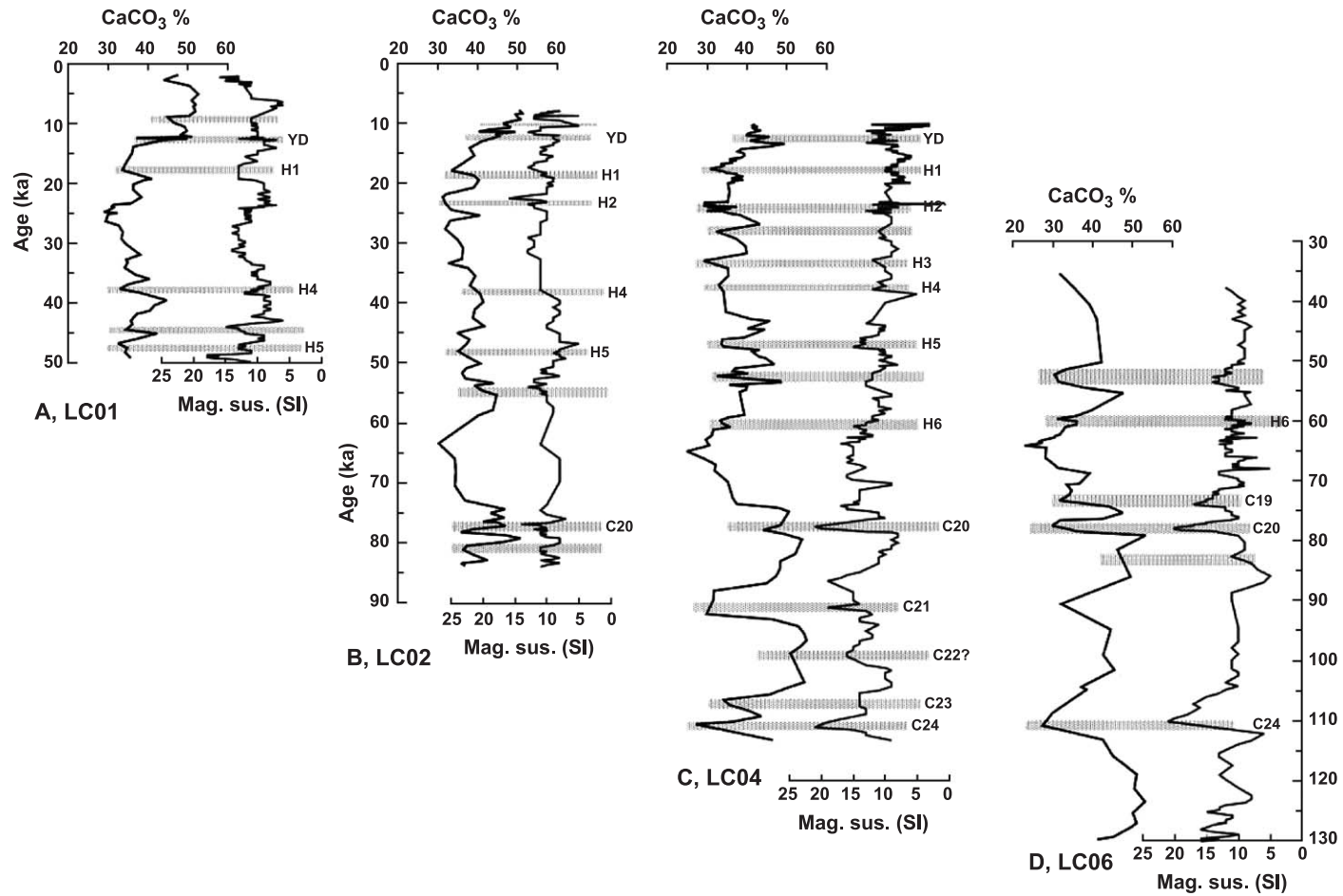


Fig. 6. Calcium carbonate contents (%) and magnetic susceptibility plotted against age (ka BP) for LC01 (A), LC02 (B), LC04 (C), and LC06 (D). Also noted are conspicuous short-term CaCO_3 lows that coincide with enhanced magnetic susceptibility values (grey shading). The timing of these short-term events seems to correspond to the timing of cold events in the North Atlantic: Hs indicates Heinrich events; Cs indicates cold events within MIS 5 (Johnsen et al., 1992; Bond et al., 1993; McManus et al., 1994; Bond and Lotti, 1995; Chapman and Shackleton, 1999; Lehman et al., 2002).

component [mainly quartz (silt and rare fine sand) and clay, with rare calcite, dolomite, mica, and feldspar]. Most silt-sized quartz particles have chipped and/or frosted surfaces, with some particles showing haematitic stains. Siliceous bioclasts (e.g., radiolarian and diatoms) appear rare in all hemipelagic sediments and commonly make up less than 2%.

The clay mineral composition of the <2- μm fraction was determined for 22 hemipelagic samples. All samples contained the following clay minerals: illite, expandable clay minerals (smectite and illite–smectite), chlorite, and kaolinite. Illite is the predominant clay (making up 32–51% of the total clay), and chlorite and kaolinite contents are approximately equal (both ~8% of the total clays). Some of the expandable clay minerals show a broad superlattice, indicating the presence of some illite–smectite mixed-layer clay mineral. No discrete secondary smectite–illite peak was identified; therefore, the expandable clay minerals are regarded as a mixture of smectite and illite–smectite of variable composition. Palygorskite, a characteristic Saharan dust mineral (Chamley, 1971; Coudé-Gaussen and Blanc, 1985), may be present in very small amounts, but dilution with other clay minerals may mask its presence in Balearic Abyssal Plain hemipelagic sediments.

7. Discussion

7.1. Glacial/interglacial CaCO_3 cycles in the Balearic Abyssal Plain

Hemipelagic CaCO_3 records for the Balearic Abyssal Plain show trends that are similar to those found in the Atlantic, with low CaCO_3 contents (~30%) during glacial periods and high CaCO_3 contents (~50%) during interglacials (Fig. 3). In the Atlantic, these CaCO_3 cycles are caused by increased dilution with terrigenous wind-blown material (Broecker et al., 1958; Ruddiman, 1971; Hays and Perruzza, 1972). At other sites in the western Mediterranean, CaCO_3 changes have been attributed to a combination of variations in productivity and dilution with terrigenous sediments (Van Os et al., 1994; Flores et al., 1997).

As discussed earlier, the CaCO_3 content of deep-sea sediments is generally controlled by three factors,

including dissolution, surface water productivity, and dilution. Dissolution does not play a major role in the four cores studied, as microscopic (light and scanning electron microscopy) examination showed that the calcareous nannoplankton and foraminiferal assemblages (from both glacial and interglacial intervals) are generally abundant, well preserved, and diverse. The $\delta^{13}\text{C}$ values (not shown) throughout the cores are relatively uniform, suggesting only a limited impact of carbonate productivity. Dilution by increased non-carbonate productivity (in the form of opal) is probably of minor importance, as diatoms and radiolarians make up less than 2% of the sediments during all periods studied. The terrigenous fraction of the hemipelagic intervals studied contains varying proportions of both clay and silt with some very fine sand-sized material (Fig. 7). Glacial intervals have a 1.5–2 times higher total terrigenous contribution (mainly silt and clay+some very fine sand) compared to interglacial intervals (Fig. 7). The clay contribution varies between 2.5% and 22% and lower values are observed during cold intervals (Fig. 7). On the other hand, the terrigenous silt/very fine sand contribution seems generally higher (10–26%), and this size fraction is especially enhanced during cold intervals (Fig. 7).

Enhanced magnetic susceptibility values (Fig. 6) and increased influx of terrigenous particles during glacial periods (Fig. 7) suggest that the Balearic Abyssal Plain carbonate cycles are most likely the result of changes in dilution with terrigenous materials. Thus, elevated hemipelagic accumulation rates recorded during low to intermediate CaCO_3 intervals coincident with MIS 2, MIS 3, and MIS 4 may result from increased dilution with terrigenous particles, with the highest rates recorded for MIS 2 and MIS 4 (Figs. 6 and 8). Weldeab et al. (2003) observed similar trends on the southern flank of Menorca, and found that terrigenous sediment accumulation rates were three to six times higher during glacial periods (MIS 2 and MIS 4) than during interglacial periods (MIS 1 and MIS 5).

In Saharan dust, kaolinite commonly exceeds the amount of chlorite (Chester et al., 1977; Guerzoni et al., 1997); thus, a kaolinite/chlorite ratio >2 in clay minerals may indicate a dominance of Saharan dust, whereas a ratio <2 may indicate input from other sources areas (Fig. 9). The kaolinite/chlorite ratio of

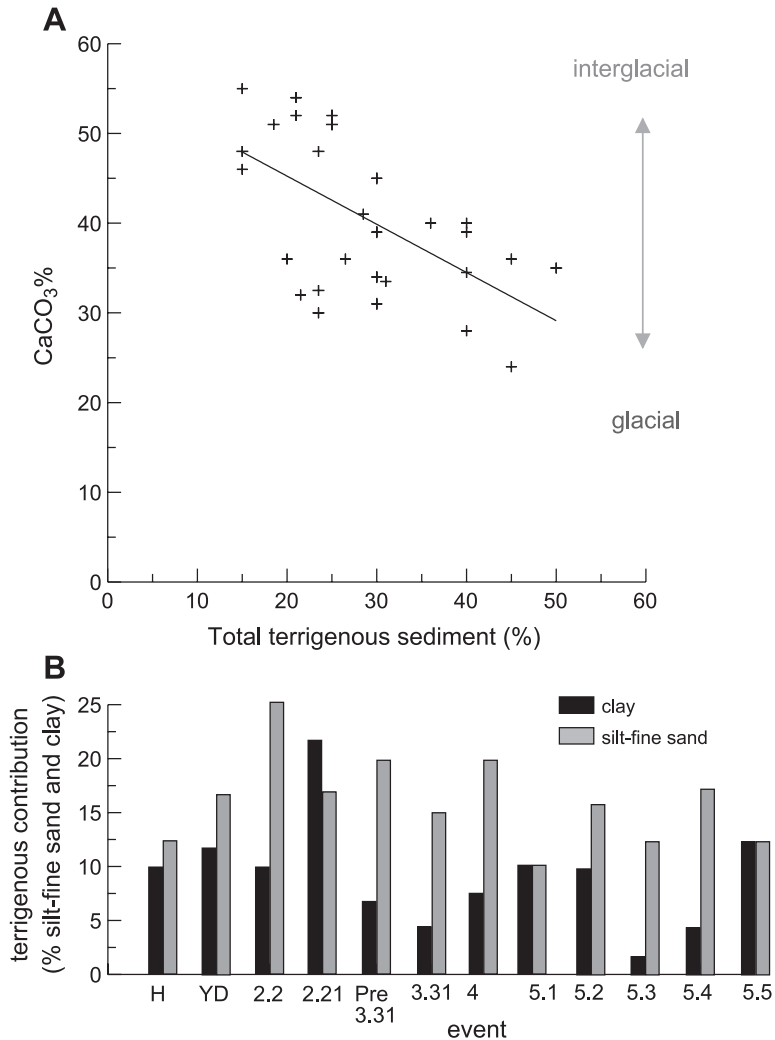


Fig. 7. (A) Relationship between CaCO₃ content (%), measured by coulometry, and the total terrigenous particle contribution (clay and silt to fine sand) in hemipelagic intervals in the four cores. The terrigenous content was estimated using percentage estimation comparison charts (Rothwell, 1989) and has not been scaled to make 100%. (B) The average terrigenous contribution (%) of clay and terrigenous silt to very fine silt in hemipelagic interval as estimated for the Holocene, Younger Dryas (YD), and oxygen isotope events 2.2, 2.21, 3.31, 4.22, 5.1, 5.2, 5.3, 5.4, and 5.5, and the low CaCO₃ interval following event 3.31 (see Fig. 3).

clays in hemipelagic samples from the Balearic Abyssal Plain is generally 1 or less, and is similar to that found in European-sourced atmospheric background dust and in most Balearic Abyssal Plain turbidite muds (Fig. 9). (In turbidite mud, samples with a kaolinite/chlorite ratio >1 may reflect a North African source area.) European-derived ‘background’ dust lacks appreciable smectite (Guerzoni et al., 1997). Hemipelagic clay samples from the Balearic Abyssal Plain, however, contain some form of

smectite and/or illite/smectite, and their (illite/smectite+smectite)/illite ratio (0.5–1) is similar to those of turbidite muds (Fig. 9).

The uniformity of clay minerals in the hemipelagic intervals and their similarity to clay minerals found in the turbidite muds (Fig. 9) suggest that the majority of the clays are derived from a common non-aeolian ‘source area.’ The presence of aeolian-derived clays in the basin is most likely masked as a result of dilution with these non-aeolian clays. The basin turbidites

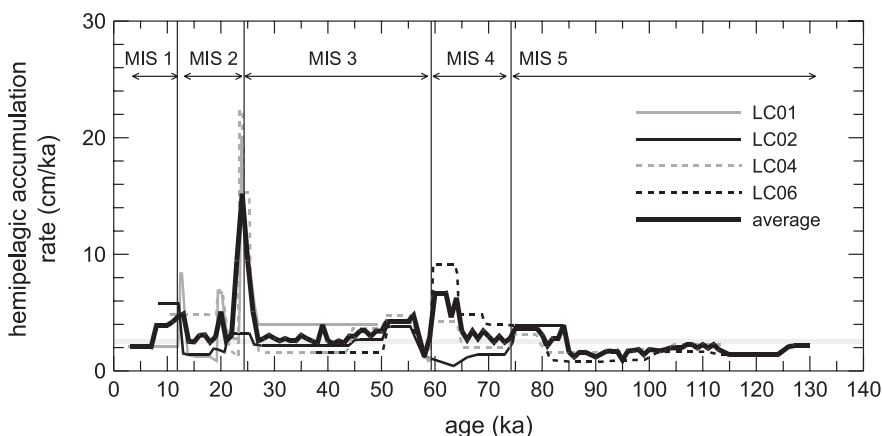


Fig. 8. Calculated hemipelagic accumulation rates for the summed hemipelagic intervals in the four long piston cores. Corrected hemipelagic depths were used for this calculation. MIS (MIS 1–5) are also indicated. The average hemipelagic accumulation rate (~ 2.5 cm/ka) is indicated by a thick grey line.

mainly originate from the southern European margin (turbidite bases towards the northern part of the basin are thicker and coarser in grain size), which receives large amounts of fluvial sediment from the rivers Ebro, Rhône, and Var. Suspended fluvially derived

material can be transported offshore by surface and/or deep currents. Surface currents are unlikely to carry suspended material into the open western Mediterranean, as surface circulation is mainly in an anticlockwise direction along the continental slope (Beckers et

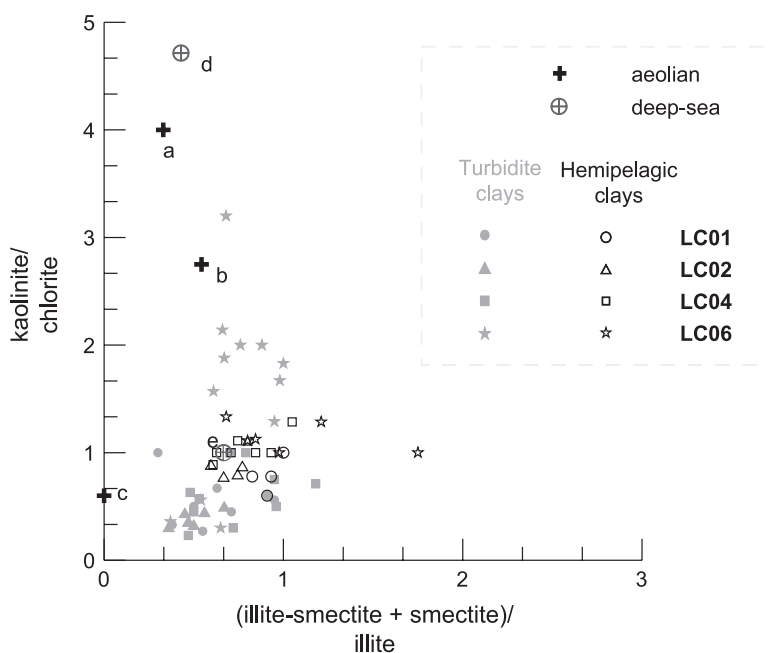


Fig. 9. Kaolinite/chlorite and (smectite+illite–smectite)/illite ratios for hemipelagic and turbidite clay minerals from the Balearic Abyssal Plain. Similar ratios are also shown for Saharan dust measured in Sardinia (a) and the NE Mediterranean (b), European background dust (c), and deep-sea sediments from the southern Tyrrhenian (d) and the south Adriatic (e) (Chester et al., 1977; Guerzoni et al., 1997).

al., 1997; Millot, 1999). Tyrrhenian Deep Water (between 600 and 1600–1900 m water depth) and Western Mediterranean Deep Water (<1900 m), on the other hand, may flow in a southerly direction (Rhein et al., 1999; Cacho et al., 2000) and could provide transport mechanisms capable of delivering suspended sediment to the open sea from the southern European margin. Bryden and Stommel (1982) and Wu and Haines (1998) suggest that Western Mediterranean Deep Water contributes to the Strait of Gibraltar outflow (Bryden and Stommel, 1982; Wu and Haines, 1998), perhaps as a result of large-scale spreading by eddy circulation (Testor and Gascard, 2003).

At present, there is only limited information on the presence and strength of deep-sea currents flowing southward from the southern European margin, and it is unclear whether they are capable of transporting coarser terrigenous particles (up to very fine sand) to the open western Mediterranean. The presence of rare calcite, dolomite, and feldspar in this size fraction could be indicators of southern (North African) aeolian dust (Tomadin and Lenaz, 1989). However, these minerals are also present in the Rhône terrigenous load (Chamley, 1971). Some of the quartz grains in the silt/very fine sand fraction show haemititic stains and/or frosted surfaces, which may be indicators of aeolian transport.

During cold intervals, the silt/fine sand fraction appears much higher proportionately than the clay fraction, whereas during warm intervals, they appear approximately equal (Fig. 7). Although it cannot be completely excluded, it seems unlikely that the increased coarser terrigenous fraction recorded during glacial intervals is transported southward by deep-sea currents from the southern European margin. Winnowing due to increased Mediterranean deep water formation and circulation during glacials seems unlikely, as this requires fairly high bottom current speed. Furthermore, there are no indicators of winnowing throughout the studied cores. Planktonic foraminifera appear well preserved with only a few fragments, benthic foraminifera are very rare (<1% of total sediment), and benthic shallow water species are absent. The increase in the coarser fraction seen in hemipelagic intervals during cold periods, therefore, may be best explained by enhanced aeolian sediment input to

the basin (Fig. 7). This suggests that a glacial increase in fine terrigenous sediment (clay to fine silt) could be from both aeolian and fluvial sources, whereas any coarser material is more likely of an aeolian origin.

The increase in aeolian sediment input during glacial periods may result from intensified and more frequent dust input into the western Mediterranean Sea. Higher aridity and/or high wind speeds during glacials can be attributed to a more southward migration of the average location of the intertropical convergence zone (ITCZ) (Matthewson et al., 1995; Weldeab et al., 2003). Further evidence for changes in the prevailing atmospheric circulation over the basin is reflected in changes in the predominant aeolian sediment source area; from Morocco/western Algeria and Tunisia/western Libya during interglacials to the Sahara/Sahelian region; and an unknown sediment source during glacials (Weldeab et al., 2003). Based on the abundance of *Cedrus* pollen in marine cores located north of Morocco, Magri and Parra (2002) show that winds frequently were northern over North Africa during the last glacial period, which were likely to carry dust. Pollen sequences from western and central Mediterranean countries and marine sites show dramatic changes during interglacial/glacial cycles (Combourieu Nebout et al., 2002; Magri and Parra, 2002). Interglacial forest-dominated flora, reflecting warm and moist climatic conditions, were replaced by open or open forest-type vegetation characteristic of a steppe/semidesert environment during glacial intervals, suggesting drier and colder climatic conditions (Combourieu Nebout et al., 2002; Magri and Parra, 2002). As climate in the western Mediterranean borderlands became more arid during the last glacial (Elenga et al., 2000), soil erosion and enhanced aeolian transport would have contributed to the increased dust flux to the western Mediterranean.

Apart from enhanced aeolian sediment transport, it is likely that the colder and drier glacial conditions would have caused increased erosion and fluvial sediment transport, combined with a highly peaked river discharge. In addition, low sea level would result in continental shelves being exposed as subareal coastal plains, allowing rivers to dump their sediment loads closer to the shelf edge, thus promoting increased fluvial input of fine terrigenous sediment into the basin.

The two cold MIS substages (MISs), 5d and 5b, within MIS 5, also show reduced CaCO_3 contents and higher magnetic susceptibility values compared with the warmer MISs 5e, MISs 5c, and MISs 5a (see Fig. 3), suggesting they may have increased terrigenous sediment input. Clay and silt to fine sand-sized terrigenous contributions are generally similar during MISs 5e and MISs 5a, whereas the silt to very fine sand contributions are higher compared to contribution of the clay fraction during MISs 5d, MISs 5c, and MISs 5b (Fig. 7). Higher contributions of terrigenous sediment during cold MISs 5d and MISs 5b confirm that the recorded lower CaCO_3 contents may be the result of increased dilution (Fig. 7). The increase in the coarser fraction (coarse silt to very fine sand) during MISs 5d and MISs 5b is likely the result of increased aeolian sediment input into the basin. Locally, sediment and soil sequences along the northeastern coast of Mallorca record aeolian deposition during MISs 5d and MISs 5b due to drier climate regimes and low biomass, whereas MISs 5e and possibly MISs 5c and MISs 5a are characterised by soil formation associated with high moisture regimes and an extensive vegetation cover (Rose et al., 1999).

7.2. Short-term CaCO_3 trends in the western Mediterranean pelagic sediments

As discussed earlier, several short-term (duration ~500–2000 years) CaCO_3 lows can be identified coincident with elevated magnetic susceptibility values within hemipelagic intervals (Fig. 6). Many of these short-term CaCO_3 fluctuations record the lowest CaCO_3 values, suggesting that they represent episodes of most pronounced dilution with terrigenous sediment in the Balearic Abyssal Plain (Fig. 6). These pronounced dilution ‘maxima’ may be the result of very severe (dry and cold) climatic conditions in the Mediterranean borderlands, causing increased aridity and dramatic increases in aeolian and fluvial sediment transport. The timing of these events appears coincident with short-term cooling phases that have been recorded in North Atlantic deep-sea sediments (Johnsen et al., 1992; Bond et al., 1993; McManus et al., 1994; Bond and Lotti, 1995; Chapman and Shackleton, 1999; Lehman et al., 2002), such as the Younger Dryas, HEs, some D/O stadials, and abrupt cooling

events within MIS 5. Most D/O stadials, however, are not obvious from the records (Fig. 6). These events may either not be recorded (signals may have been smoothed due to only moderate sedimentation rates combined with bioturbation, or the hemipelagic substrate may have been eroded by turbidity currents), or climate during D/O stadials in the western Mediterranean Sea may not have been as severe as in the Atlantic.

Elevated aeolian input into the basin during these short-term cold events may be explained by intensified high-latitude circulation and a weakened monsoonal circulation causing greater Saharan wind intensities, resulting in increased northward dust transport (Moreno et al., 2002; Rohling et al., 2003). Fluvial sediment input (clay to very fine silt) was probably also increased during HEs. Expansion of the polar vortex may have resulted in cooling of the NE Mediterranean due to more frequent and intense outbreaks of polar/continental air (Rohling et al., 1998, 2003), causing increased deep-water formation (Cacho et al., 2000) that could promote the southward transport of fine (clay and very fine silt) terrigenous sediment.

Pollen records from terrestrial lacustrine sequences at various sites in the Mediterranean confirm that continental climatic conditions in the Mediterranean during HEs and D/O stadials were dry and can be linked to climatic conditions in the North Atlantic (Allen et al., 1999, 2000; Tzedakis, 1999; Allen and Huntley, 2000; Brauer et al., 2000). In the Alboran Sea, pollen records show vegetation changes that are indicative of rapid environmental changes between cold-dry (D/O stadials) and mild-humid conditions (D/O interstadials) (Comboureu Nebout et al., 2002), which occur in parallel with SST oscillations and indicate an almost perfect coupling between continental and marine conditions (Sánchez Goñi et al., 2002). The coldest and driest conditions in the Alboran Sea occurred during HEs (Comboureu Nebout et al., 2002; Sánchez Goñi et al., 2002) and similar conditions may have prevailed in the Balearic Basin, as HEs-related trends seem more apparent than D/O stadials in our cores (Fig. 6). Less pronounced decreases in precipitation during D/O stadials may be explained by switches between the influence of moister Atlantic (dominant during D/O stadials) and colder/drier Scandinavian

Mobile Polar Highs (dominant during HEs) (Sánchez Goñi et al., 2002). Mobile Polar Highs are considered to be the key factor of meridional air exchange (Leroux, 1993) and the development of a substantial Scandinavian Mobile Polar High during HEs may have resulted in prolonged wintertime anticyclonic activity, causing increased aridity and desertification in the Mediterranean region (Combourieu Nebout et al., 2002).

8. Conclusions

Although late Quaternary sediments on the Balearic Abyssal Plain are dominated by turbidite deposits, an almost continuous record of hemipelagic sedimentation covering the last 130,000 years is preserved in the intercalated intervals. Analysis of calcium carbonate content of these hemipelagic sediments reveals distinct cycles similar to ‘Atlantic’-type carbonate cycles; with interglacial periods showing relatively higher CaCO₃ contents (~50%) and glacial periods showing lower CaCO₃ contents (~30%). AMS radiocarbon dating, biostratigraphy (based on coccolith intervals), and oxygen isotope stratigraphy support the time relationship inferred from this climatic pattern in the calcium carbonate contents. Enhanced magnetic susceptibility values and increased contributions of terrigenous material during glacial periods suggest that the Balearic Abyssal Plain carbonate cycles are most likely the result of changes in dilution with terrigenous particles. Clay mineral analyses show that clays in the hemipelagic intervals are mainly derived from the southern European margin and are most likely transported to the open western Mediterranean Sea by deep currents and/or eddy advection. Coarser-grained terrigenous particles (coarse silt and very fine sand), on the other hand, may be too heavy to be transported in a similar manner; instead, it is suggested that aeolian processes may be responsible for their delivery to the basin plain.

The increases in aeolian sediment transport to the western Mediterranean Sea may result from changes in the prevailing atmospheric conditions, causing colder and drier climatic conditions in the source areas and more frequent and intense outbreaks of aeolian dust transport. In addition, glacial conditions

probably also caused an increase in fluvial sediment transport with a highly peaked river discharge. Lower sea level would have facilitated delivery of this sediment to the deep sea, as rivers would have discharged close to the present shelf edge.

Several ‘short-term’ CaCO₃ lows can be identified in the four cores that appear coincident with elevated magnetic susceptibility values. The timing of these short-term trends can be linked with cooling events in the North Atlantic, and can also be explained by increased terrigenous dilution. They are interpreted as possibly reflecting more drier and colder climatic conditions in the Mediterranean borderlands, resulting in increased aeolian and fluvial sediment transport.

Acknowledgements

We acknowledge valuable reviews by Christian Robert, Bill Ruddiman and an anonymous reviewer. Mike Bolshaw, Steve Cooke, Matt Cooper, and Mike Rogerson are thanked for assistance with stable isotope analysis. Tracey Cummins helped with the sample preparation before oxygen and carbon isotope analysis and determined foraminiferal abundance. Darryl Green provided assistance while measuring CaCO₃ contents. Access to the studied cores was provided by the British Ocean Sediment Core Research Facility (BOSCORF) located at Southampton Oceanography Centre. We also thank John Thomson for stimulating discussions.

References

- Added, A., Fernex, E., Ringot, J.L., Span, D., 1984. Caractères sédimentologiques et géochimiques du plateau continental devant l’embouchure de grande Rhône. In: Bizon, J.J., Buvollet, P.F. (Eds.), *Ecologie des microorganismes en Méditerranée occidentale*. Association Française des Techniques du Pétrole, Paris, pp. 33–45.
- Allen, J.R.M., Huntley, B., 2000. Weichselian palynological records from southern Europe: correlation and chronology. *Quat. Int.* 73/74, 111–125.
- Allen, J.R.M., Brandt, U., Brauer, A., Hubberten, H.-W., Huntley, B., Keller, J., Kraml, M., Mackensen, A., Mingram, J., Negendank, J.F.W., Nowaczyk, N.R., Oberhansli, H., Watts, W.A., Wulf, S., Zolitschka, B., 1999. Rapid environmental changes in southern Europe during the last glacial period. *Nature* 400, 740–742.

- Allen, J.R.M., Watts, W.A., Huntley, B., 2000. Weichselian palynostratigraphy, palaeovegetation and palaeoenvironment; the record from Lago Grande di Monticchio, southern Italy. *Quat. Int.* 73/74, 91–110.
- Alonso, B., Maldonado, A., 1990. Late Quaternary sedimentation patterns of the Ebro turbidite system (northwestern Mediterranean): Two styles of deep-sea deposition. *Mar. Geol.* 95, 353–377.
- Amerigian, C., 1974. Sea-floor dynamic processes as the possible cause of correlation between paleoclimate and paleomagnetic indices in deep-sea sedimentary cores. *Earth Planet. Sci. Lett.* 21, 321–326.
- Avila, A., Queralt-Mitjans, I., Alarcón, M., 1997. Mineralogical composition of African dust delivered by red rains over northeastern Spain. *J. Geophys. Res.* 102, 21977–21996.
- Bárcena, M.A., Cacho, I., Abrantes, F., Sierro, F.J., Grimalt, J.O., Flores, J.A., 2001. Paleoproductivity variations related to climatic conditions in the Alboran Sea (western Mediterranean) during the last glacial–interglacial transition: the diatom record. *Palaeogeogr. Palaeoclimatol. Palaeoecol.* 167, 337–357.
- Beckers, J.-M., Brasseur, P., Nihoul, C.J., 1997. Circulation of the western Mediterranean: from global to regional scales. *Deep-Sea Res. II* 44, 531–549.
- Bellaiche, G., 1993. Sedimentary mechanisms and underlying tectonic structures of the northwestern Mediterranean margin, as revealed by comprehensive bathymetric and seismic surveys. *Mar. Geol.* 112, 89–108.
- Bergametti, G., Dutot, A.L., Buat-Ménard, P., Remoudaki, E., 1989a. Seasonal variability of the elemental composition of atmospheric aerosol particles over the northwestern Mediterranean. *Tellus* 41B, 553–561.
- Bergametti, G., Gomes, L., Remoudaki, E., Desbois, M., Martin, D., Buat-Ménard, P., 1989b. Present transport and deposition patterns of African dusts to the north-western Mediterranean. In: Leinen, M., Sarnthein, M. (Eds.), *Paleoclimatology and Paleometeorology: Modern and Past Patterns of Global Atmospheric Transport*, NATO ASI Series, Mathematical and Physical Sciences, vol. 282, pp. 227–250.
- Bloemendal, J., DeMenocal, P., 1989. Evidence for a change in the periodicity of tropical climate cycles at 2.4 Myr from whole-core magnetic susceptibility measurements. *Nature* 342, 897–900.
- Bond, G.C., Lotti, R., 1995. Iceberg discharges into the North Atlantic on millennial time scales during the last glaciation. *Science* 267, 1005–1010.
- Bond, G., Broecker, W., Johnsen, S., McManus, J., Labeyrie, L., Jouzel, J., Bonani, G., 1993. Correlations between climate records from North Atlantic sediments and Greenland ice. *Nature* 365, 143–147.
- Brauer, A., Mingram, J., Frank, U., Günter, C., Schettler, G., Wulf, S., Zolitschka, B., Negendank, J.F.W., 2000. Abrupt environmental oscillations during the Early Weichselian recorded at Lago Grande di Monticchio, southern Italy. *Quat. Int.* 73/74, 79–90.
- Brindley, G.W., Brown, G. (Eds.), 1980. *Crystal Structures of Clay Minerals and Their X-ray Identification*. Mineralogical Society, London, 495 pp.
- Broecker, W.S., Turekian, K.K., Heezen, B.C., 1958. The relation of deep-sea sedimentation rates to variations in climate. *Am. J. Sci.* 256, 503–517.
- Brovkin, V., Claussen, M., Petoukhov, V., Ganopolski, A., 1998. On the stability of the atmosphere–vegetation system in the Saharan/Sahel region. *J. Geophys. Res.* 103, 31613–31624.
- Bryden, H.L., Stommel, H.M., 1982. Origin of the Mediterranean outflow. *J. Mar. Res., Suppl.* 40, 55–71.
- Bücher, A., Lucas, G., 1984. Sédimentation éolienne intercontinentale, poussières sahariennes et géologie. *Bull. Cent. Rech. Explor. Prod. Elf-Aquitaine* 8, 151–165.
- Bücher, A., Dubief, J., Lucas, C., 1983. Retombées estivales de poussières sahariennes sur l'Europe. *Rev. Géogr. Phys. Géol. Dyn.* 24, 153–165.
- Cacho, I., Grimalt, J.O., Pelejero, C., Canals, M., Sierro, F.J., Flores, J.A., Shackleton, N.J., 1999. Dansgaard–Oeschger and Heinrich event imprints in the Alboran Sea paleotemperatures. *Paleoceanography* 14, 698–705.
- Cacho, I., Grimalt, J.O., Sierro, F.J., Shackleton, N., Canals, M., 2000. Evidence for enhanced Mediterranean thermohaline circulation during rapid climatic coolings. *Earth Planet. Sci. Lett.* 183, 417–429.
- Cacho, I., Grimalt, J.O., Canals, M., Saffi, L., Shackleton, N.J., Schönfeld, J., Zahn, R., 2001. Variability of the western Mediterranean Sea surface temperature during the last 25,000 years and its connection with the Northern Hemisphere climatic changes. *Paleoceanography* 16, 40–52.
- Chamley, H., 1971. *Recherches sur la sédimentation argileuse en Méditerranée*. Thèse, Univ. Aix-Marseille. 401 pp.
- Chapman, M.R., Shackleton, N.J., 1999. Global ice-volume fluctuations, North Atlantic ice-rafting events, and deep-ocean circulation changes between 130 and 70 ka. *Geology* 27, 795–798.
- Chester, R., Baxter, G.G., Behairy, A.K.A., Connor, K., Cross, D., Elderfield, H., Padgham, R.C., 1977. Soil-sized eolian dust from the lower troposphere of the eastern Mediterranean Sea. *Mar. Geol.* 24, 201–217.
- Claussen, M., Brovkin, V., Ganopolski, A., Kubatzki, C., Petoukhov, V., 1998. Modelling global terrestrial vegetation–climate interaction. *Philos. Trans.-R. Soc. Lond.* 353, 53–63.
- Combourieu Nebout, N., Turon, J.L., Zahn, R., Capotondi, L., Londeix, L., Pahnke, K., 2002. Enhanced aridity and atmospheric high-pressure stability over the western Mediterranean during the North Atlantic cold events of the past 50 ky. *Geology* 30, 863–866.
- Coudé-Gaussen, G., Blanc, P., 1985. Présence de grains éolisés de palygorskite dans les poussières actuelles et les sédiments récents d'origine désertique. *Bull. Soc. Géol. Fr.* 8, 571–579.
- Diester-Haas, L., 1976. Late Quaternary climatic variations in northwest Africa deduced from east Atlantic sediment cores. *Quat. Res.* 6, 299–314.
- Elenga, H., Peyron, O., Bonnefille, R., Jolly, D., Cheddadi, R., Guiot, J., Andrieu, V., Bottema, S., Bucher, G., de Beaulieu, J.-L., Hamilton, A.C., Maley, J., Marchant, R., Perez-Obiol, R., Reille, M., Riollet, G., Scott, L., Straka, H., Taylor, D., Van Campo, E., Vincens, A., Laarif, F., Jonson, H., 2000. Pollen-

- based biome reconstruction for southern Europe and Africa, 18,000 yr BP. *J. Biogeogr.* 27, 621–634.
- Emiliani, C., 1955. Pleistocene temperatures. *J. Geol.* 63, 538–578.
- Flores, J.A., Sierro, F.J., Francés, G., Vázquez, A., Zamarreño, I., 1997. The last 100,000 years in the western Mediterranean: sea surface water and frontal dynamics as revealed by coccolithophores. *Mar. Micropaleontol.* 29, 351–366.
- Foucault, A., Mélières, F., 2000. Palaeoclimatic cyclicity in central Mediterranean Pliocene sediments: the mineralogical signal. *Palaeogeogr. Palaeoclimatol. Palaeoecol.* 158, 311–323.
- González-Donoso, J.M., Serrano, F., Linares, D., 2000. Sea surface temperature during the Quaternary at ODP Sites 976 and 975 (western Mediterranean). *Palaeogeogr. Palaeoclimatol. Palaeoecol.* 162, 17–44.
- Goudie, A.S., Middleton, N.J., 2001. Saharan dust storms: nature and consequences. *Earth Sci. Rev.* 56, 179–204.
- Guerzoni, S., Landuzzi, W., Lenaz, R., Quarantotto, G., Cesari, G., Rampazzo, R., Molinaroli, E., 1992. Mineral atmospheric particulate from south to northwest Mediterranean: seasonal variations and characteristics. *Water Pollut. Res. Rep.* 28, 483–493.
- Guerzoni, S., Molinaroli, E., Chester, R., 1997. Saharan dust inputs to the western Mediterranean Sea: depositional patterns, geochemistry and sedimentological implications. *Deep-Sea Res. II* 44, 631–654.
- Guerzoni, S., Chester, R., Dulac, F., Herut, B., Loye-Pilot, M.-D., Measures, C., Migon, C., Molinaroli, E., Moulin, C., Rossini, P., Saydam, C., Soudini, A., Ziveri, P., 1999. The role of atmospheric deposition in the biogeochemistry of the Mediterranean Sea. *Prog. Oceanogr.* 44, 147–190.
- Hays, J.D., Perruzza, A., 1972. The significance of calcium carbonate oscillations in eastern equatorial Atlantic deep-sea sediments for the end of the Holocene warm interval. *Quat. Res.* 2, 355–362.
- Imbrie, J., Hays, J.D., Martinson, D.G., McIntyre, A., Mix, A.C., Morley, J.J., Pisias, N.G., Prell, W.L., Shackleton, N.J., 1984. The orbital theory of Pleistocene climate: support from a revised chronology of the marine $\delta^{18}\text{O}$ record. In: Berger, A., Imbrie, J., Hays, J., Kukla, G., Salzmann, B. (Eds.), *Milankovich and Climate: Understanding Response to Astronomical Forcing*. 1. Reidel, Dordrecht, pp. 269–305.
- Johnsen, S.J., Clausen, H.B., Dansgaard, W., Fuhrer, K., Gundestrup, N., Hammer, C.U., Iversen, P., Jouzel, J., Stauffer, B., Steffensen, J.P., 1992. Irregular glacial interstadials recorded in a new Greenland ice core. *Nature* 359, 311–313.
- Jones, K.P.N., McCave, I.N., Weaver, P.P.E., 1992. Textural and dispersal patterns of thick mud turbidites from the Madeira Abyssal Plain. *Mar. Geol.* 107, 149–173.
- Kent, D.V., 1982. Apparent correlation of paleomagnetic intensity and climatic records in deep-sea sediments. *Nature* 299, 538–539.
- Kolla, V., Biscaye, P.E., Hanley, A.F., 1979. Distribution of quartz in late Quaternary Atlantic sediments in relation to climate. *Quat. Res.* 11, 261–277.
- Laj, C., Mazaud, A., Duplessy, J.-C., 1996. Geomagnetic intensity and ^{14}C abundance in the atmosphere and ocean during the past 50 kyr. *Geophys. Res. Lett.* 23, 2045–2048.
- Larrasoño, J.C., Roberts, A.P., Rohling, E.J., Winkhofer, M., Wehausen, R., 2003. Three million years of monsoon variability over the northern Sahara. *Clim. Dyn.* 21, 689–698.
- Lehman, S.J., Sachs, J.P., Crotwell, A.M., Keigwin, L.D., Boyle, E.A., 2002. Relation of subtropical Atlantic temperature, high-latitude ice rafting, deep water formation, and European climate 130,000–60,000 years ago. *Quat. Sci. Rev.* 21, 1917–1924.
- Leroux, M., 1993. The Mobile Polar High: a new concept explaining present mechanisms of meridional air-mass and energy exchanges and global propagation of palaeoclimatic changes. *Glob. Planet. Change* 7, 69–93.
- Loye-Pilot, M.-D., Martin, J.-M., Morelli, J., 1986. Influence of Saharan dust on the rainfall acidity and atmospheric input to the Mediterranean. *Nature* 321, 427–428.
- Loye-Pilot, M.-D., Martin, J.M., Morelli, J., 1989. Atmospheric input of particulate matter and inorganic nitrogen to the northwestern Mediterranean. *Water Pollut. Res. Rep.* 13, 368–376.
- Magri, D., Parra, I., 2002. Late Quaternary western Mediterranean pollen records and African winds. *Earth Planet. Sci. Lett.* 200, 401–408.
- Martin, J.-M., Elbaz-Poulichet, F., Guieu, C., Loye-Pilot, M.-D., Han, G., 1989. River versus atmospheric input of material to the Mediterranean Sea: an overview. *Mar. Chem.* 28, 159–182.
- Martinson, D.G., Pisias, N.G., Hayes, J.D., Imbrie, J., Moore, T.C., Shackleton, N.J., 1987. Age dating and the orbital theory of the ice ages: development of a high-resolution 0 to 300,000 year chronostratigraphy. *Quat. Res.* 27, 1–29.
- Matthewson, A.P., Shimmield, G.B., Kroon, D., Fallick, A.E., 1995. A 300 kyr high-resolution aridity record of the North African continent. *Paleoceanography* 10, 677–692.
- McManus, D.A., 1970. Criteria of climatic change in the inorganic components of marine sediments. *Quat. Res.* 1, 72–102.
- McManus, J.F., Bond, G.C., Broecker, W., Johnson, S., Labeyrie, L., Higgins, S., 1994. High-resolution climate records from the North Atlantic during the last interglacial. *Nature* 371, 326–329.
- Middleton, N.J., 1985. Effect of drought on dust production in the Sahel. *Nature* 316, 431–434.
- Millot, C., 1999. Circulation in the western Mediterranean Sea. *J. Mar. Syst.* 20, 423–442.
- Molinaroli, E., 1996. Mineralogical characterisation of Saharan dust with a view to its final destination in Mediterranean sediments. In: Guerzone, S., Chester, R. (Eds.), *The Impact of Desert Dust Across the Mediterranean*. Kluwer Academic Publishing, pp. 153–162.
- Moreno, A., Cacho, I., Canals, M., Prins, M.A., Sánchez-Goni, M.-F., Grimalt, J.O., Weltje, G.J., 2002. Saharan dust transport and high-latitude glacial climatic variability: the Alboran Sea record. *Quat. Res.* 58, 318–328.
- Moulin, C., Lambert, C.E., Dulac, F., Dayan, U., 1997. Control of atmospheric export of dust from North Africa by the North Atlantic Oscillation. *Nature* 387, 691–694.
- Mulder, T., Savoye, B., Syvitski, J.P.M., Parize, O., 1997. Hyperpycnal turbidite currents at the head of the Var Canyon? Hydrological data and geological observations. *Oceanol. Acta* 20, 607–626.

- Nelson, C.H., 1990. Estimated post-Messinian sediment supply and sedimentation rates on the Ebro continental margin. Spain. *Mar. Geol.* 95, 395–418.
- Oldfield, F., Robinson, S.G., 1985. Geomagnetism and palaeoclimate. In: Tooley, M.J., Sheil, G.M. (Eds.), *The Climatic Scene*. Allen & Unwin, Winchester, MA, pp. 186–205.
- Parkin, D.W., 1974. Trade winds during glacial cycles. *Proc. R. Soc.* 337, 73–100.
- Parkin, D.W., Shackleton, N.J., 1973. Trade wind and temperature correlations down a deep-sea core off the Saharan coast. *Nature* 245, 455–457.
- Paterne, M., Kallel, N., Labeyrie, L., Vautravers, M., Duplessy, J.C., Rossignol-Strick, M., Cortijo, E., Arnold, M., Fontugne, M., 1999. Hydrological relationship between the North Atlantic Ocean and the Mediterranean Sea during the past 15–75 kyr. *Paleoceanography* 14, 626–638.
- Pont, D., 1993. Vers une Meilleures Connaissance des Apports du Rhône à la Méditerranée. Les rencontres de l'Agence Régionale Pour l'Environnement. Région PACA (Provence, Alpes Côte d'Azur), 16–24.
- Prell, W.L., Imbrie, J., Martinson, D.G., Morley, J.J., Pisias, N.G., Shackleton, N.J., Streeter, H.F., 1986. Graphic correlation of oxygen isotope stratigraphy application to the late Quaternary. *Paleoceanography* 1, 137–162.
- Prentice, I.C., Guiot, J., Harrison, S.P., 1992. Mediterranean vegetation, lake levels and palaeoclimate at the last glacial maximum. *Nature* 360, 658–660.
- Rhein, M., Send, U., Klein, B., Krahnmann, G., 1999. Interbasin deep water exchange in the western Mediterranean. *J. Geophys. Res.* 104, 23495–23508.
- Robinson, S.G., 1986. The late Pleistocene palaeoclimatic record of North Atlantic deep-sea sediments revealed by mineral magnetic measurements. *Phys. Earth Planet. Inter.* 42, 22–57.
- Robinson, S.G., Maslin, M.A., McCave, I.N., 1995. Magnetic susceptibility variations in Upper Pleistocene deep-sea sediments of the NE Atlantic: implications for ice rafting and paleocirculation at the last glacial maximum. *Paleoceanography* 10, 221–250.
- Rognon, P., 1987. Aridification and abrupt climatic events on the Saharan northern and southern margins, 20,000 years BP to present. In: Berger, W.H., Labeyrie, C.D. (Eds.), *Abrupt Climatic Change: Evidence and Implications*. Reidel, Dordrecht, pp. 209–220.
- Rohling, E.J., Hayes, A., de Rijk, S., Kroon, D., Zachariasse, J.W., 1998. Abrupt cold spells in the NW Mediterranean. *Paleoceanography* 13, 316–322.
- Rohling, E.J., Mayewski, P.A., Challenor, P., 2003. On the timing and mechanism of millennial-scale climate variability during the last glacial cycle. *Clim. Dyn.* 20, 257–267.
- Rose, J., Meng, X., Watson, C., 1999. Palaeoclimate and palaeoenvironment responses in the western Mediterranean over the last 140 ka: evidence from Mallorca, Spain. *J. Geol. Soc.* 156, 435–448.
- Rothwell, R.G., 1989. Minerals and Mineraloids in Marine Sediments: An Optical Identification Guide. Elsevier, London. 279 pp.
- Rothwell, R.G., Weaver, P.P.E., Hodkinson, R.A., Pratt, C.E., Styzen, M.J., Higgs, N.C., 1994. Clayey nannofossil ooze turbidites and hemipelagites at Sites 834 and 835 (Lau Basin, Southwest Pacific). In: Hawkins, J., Parson, L., Allen, J., et al. (Eds.), *Proc. Ocean Drill. Program Sci. Results*, vol. 135, pp. 101–130.
- Rothwell, R.G., Thomson, J., Kähler, G., 1998. Low-sea-level emplacement of a very large Late Pleistocene 'megaturbidite' in the western Mediterranean Sea. *Nature* 392, 377–380.
- Rothwell, R.G., Reeder, M.S., Anastasakis, G., Stow, D.A.V., Thomson, J., Kähler, G., 2000. Low sea-level stand emplacement of megaturbidites in the western and eastern Mediterranean Sea. *Sediment. Geol.* 135, 75–88.
- Ruddiman, W.F., 1971. Pleistocene sedimentation in the equatorial Atlantic: stratigraphy and faunal paleoclimatology. *Geol. Soc. Am. Bull.* 82, 283–302.
- Rupke, N.A., Stanley, D.J., 1974. Distinctive properties of turbidite and hemipelagic mud layers in the Algéro-Balearic Basin, western Mediterranean Sea. *Smithson. Contrib. Earth Sci.* 13, 1–40.
- Sánchez Goñi, M.F., Cacho, I., Turon, J.-L., Guiot, J., Sierro, F.J., Peyrouquet, J.-P., Grimalt, J.O., Shackleton, N.J., 2002. Synchronicity between marine and terrestrial responses to millennial scale climatic variability during the last glacial period in the Mediterranean region. *Clim. Dyn.* 19, 95–105.
- Shackleton, N.J., Opdyke, N.D., 1973. Oxygen isotope and paleomagnetic stratigraphy of Equatorial Pacific Core V28-238: oxygen isotope temperatures and ice volumes on a 10^5 year and 10^6 year scale. *Quat. Res.* 3, 39–55.
- Stow, D.A.V., Piper, D.J.W., 1984. Deep-water fine-grained sediments: facies models. In: Stow, D.A.V., Piper, D.J.W. (Eds.), *Fine-Grained Sediments: Deep-Water Processes and Facies*, vol. 15, pp. 611–645.
- Stow, D.A.V., Shanmugam, G., 1980. Sequence of structures in fine-grained turbidites; comparison of recent deep-sea and ancient flysch sediments. *Sediment. Geol.* 25, 23–42.
- Stow, D.A.V., Tabrez, A.R., 1998. Hemipelagites: processes, facies and model. In: Stoker, M.S., Evans, D., Cramp, A. (Eds.), *Geological Processes on Continental Margins: Sedimentation, Mass-Wasting and Stability*, Geological Society, London, Special Publication, vol. 129, pp. 317–337.
- Stuiver, M., Reimer, P.J., Bard, E., Beck, J.W., Burr, G.S., Hughen, K.A., Kromer, B., McCormac, G., Van der Plicht, J., Spurk, M., 1998. INTCAL98 radiocarbon age calibration 24,000–0 cal BP. *Radiocarbon* 40, 1041–1083.
- Testor, P., Gascard, J.-C., 2003. Large-scale spreading of deep waters in the western Mediterranean by submesoscale coherent eddies. *J. Phys. Oceanogr.* 33, 75–87.
- Thomson, J., Nixon, S., Summerhayes, C.P., Rohling, E.J., Schönfeld, J., Zahn, R., Grootes, P., Abrantes, F., Gaspar, L., Vaquero, S., 2000. Enhanced productivity on the Iberian margin during glacial/interglacial transitions revealed by barium and diatoms. *J. Geol. Soc.* 157, 667–677.
- Thouveny, N., Moreno, E., Delanghe, D., Candon, L., Lancelot, Y., Shackleton, N.J., 2000. Rock magnetic detection of distal ice-

- rafted debris: clue for the identification of Heinrich layers on the Portuguese margin. *Earth Planet. Sci. Lett.* 180, 61–75.
- Tomadin, L., Lenaz, R., 1989. Eolian dust over the Mediterranean and their contribution to the present sedimentation. In: Leinen, M., Sarnthein, M. (Eds.), *Paleoclimatology and Paleometeorology: Modern and Past Patterns of Global Atmospheric Transport*, NATO Adv. Stud. Inst. Ser., Ser. C Math. Phys. Sci., vol. 282. Dordrecht Kluwer Academic, pp. 267–282.
- Torres, J., Droz, L., Savoye, B., Terentieva, E., Cochonat, P., Kenyon, N.H., Canals, M., 1997. Deep-sea avulsion and morphosedimentary evolution of the Rhône Fan Valley and Neofan during the Late Quaternary (north-western Mediterranean Sea). *Sedimentology* 44, 457–477.
- Tzedakis, C., 1999. The last climatic cycle at Kopais, central Greece. *J. Geol. Soc. (Lond.)* 156, 425–434.
- Vanney, J.-R., Genneseaux, M., 1985. Mediterranean seafloor features: overview and assessment. In: Stanley, D.J., Wezel, F.-C. (Eds.), *Geological Evolution of the Mediterranean Basin: Raimondo Selli Commemorative Volume*. Springer-Verlag, New York, pp. 2–32.
- Van Os, B.J.H., Lourens, L.J., Hilgen, F.J., de Lange, G.J., Beaufort, L., 1994. The formation of Pliocene sapropels and carbonate cycles in the Mediterranean: diagenesis, dilution and productivity. *Paleoceanography* 9, 601–617.
- Verosub, K.L., Roberts, A.P., 1995. Environmental magnetism: past, present and future. *J. Geophys. Res.* 100, 2175–2192.
- Weaver, P.P.E., 1983. An integrated stratigraphy of the Upper Quaternary of the King's Trough flank area NE Atlantic. *Oceanol. Acta* 6, 451–456.
- Weaver, P.P.E., Thomson, J., 1993. Calculating erosion by deep-sea turbidity currents during initiation and flow. *Nature* 364, 136–138.
- Weldeab, S., Siebel, W., Wehausen, R., Emeis, K.-C., Schmiedl, G., Hemleben, C., 2003. Late Pleistocene sedimentation in the Western Mediterranean Sea: implications for productivity changes and climatic conditions in the catchment areas. *Palaeogeogr. Palaeoclimatol. Palaeoecol.* 190, 121–137.
- Wu, P., Haines, K., 1998. The general circulation of the Mediterranean Sea from a 100-year simulation. *J. Geophys. Res.* 103, 1121–1135.